The Journal of Immunology

RESEARCH ARTICLE | AUGUST 15 2018

Role of Peptidylarginine Deiminase 4 in Neutrophil Extracellular Trap Formation and Host Defense during *Klebsiella pneumoniae*–Induced Pneumonia-Derived Sepsis FREE

Theodora A. M. Claushuis; ... et. al

J Immunol (2018) 201 (4): 1241–1252.
https://doi.org/10.4049/jimmunol.1800314

Role of Peptidylarginine Deiminase 4 in Neutrophil Extracellular Trap Formation and Host Defense during *Klebsiella pneumoniae*–Induced Pneumonia-Derived Sepsis

Theodora A. M. Claushuis,* Lieve E. H. van der Donk,* Anna L. Luitse,* Henk A. van Veen,† Nicole N. van der Wel,† Lonneke A. van Vught,* Joris J. T. H. Roelofs,‡ Onno J. de Boer,‡ Jacqueline M. Lankelma,* Louis Boon,§ Alex F. de Vos,* Cornelis van 't Veer,* and Tom van der Poll*,¶

Peptidylarginine deiminase 4 (PAD4) catalyzes citrullination of histones, an important step for neutrophil extracellular trap (NET) formation. We aimed to determine the role of PAD4 during pneumonia. Markers of NET formation were measured in lavage fluid from airways of critically ill patients. NET formation and host defense were studied during pneumonia-derived sepsis caused by *Klebsiella pneumoniae* in PAD4$^{+/+}$ and PAD4$^{-/-}$ mice. Patients with pneumosepsis, compared with those with nonpulmonary disease, showed increased citrullinated histone 3 (CitH3) levels in their airways and a trend toward elevated levels of NET markers cell-free DNA and nucleosomes. During murine pneumosepsis, CitH3 levels were increased in the lungs of PAD4$^{+/+}$ but not of PAD4$^{-/-}$ mice. Combined light and electron microscopy showed NET-like structures surrounding *Klebsiella* in areas of CitH3 staining in the lung; however, these were also seen in PAD4$^{-/-}$ mice with absent CitH3 lung staining. Moreover, cell-free DNA and nucleosome levels were mostly similar in both groups. Moreover, *Klebsiella* and LPS could still induce NETosis in PAD4$^{-/-}$ neutrophils. Both groups showed largely similar bacterial growth, lung inflammation, and organ injury. In conclusion, these data argue against a major role for PAD4 in NET formation, host defense, or organ injury during pneumonia-derived sepsis. ***The Journal of Immunology*****, 2018, 201: 1241–1252.**

With a high incidence and significant mortality rate worldwide, sepsis remains a global health care problem despite antibiotic treatment and, in the developed world, access to intensive care facilities (1). Pneumonia is the most frequent site of origin for sepsis (2). Aerobic Gram-negative bacteria are the most common pathogens isolated in patients with nosocomial pneumonia and a frequent cause of sepsis (1, 3). *Klebsiella pneumoniae* is especially worrisome in this context, considering its increasing resistance to antimicrobial agents (3).

Peptidylarginine deiminase 4 (PAD4), an enzyme that catalyzes citrullination of histones, is expressed by immune cells and localizes in the nucleus and cytoplasmic granules (4, 5). PAD4 can impact immune cell function in multiple ways: for example, by influencing hematopoiesis (6), cytokine production (7, 8), and apoptosis (9). PAD4 has moreover been reported to regulate neutrophil extracellular trap (NET) formation (10, 11). NETs are released by activated neutrophils and consist of DNA, histones, proteases, and antimicrobial proteins (12). Citrullination of histone 3 (H3) by PAD4 results in weakening of DNA–histone binding, thereby facilitating the release of DNA outside the nucleus (10, 13). Although several investigations have implicated PAD4 in NETosis (10, 11, 14, 15), others have suggested that PAD4 might not be crucial for this process (16, 17), and a recent study showed that inhibition of PAD4 does not influence NETosis despite reduced citrullination of H3 (18).

During sepsis, NETs can be a part of protective immunity through their capacity to trap and kill bacteria (11) but, in contrast, can be detrimental to the host via induction of collateral tissue injury (19) and microvascular thrombosis (19, 20).

Although previous studies have examined NETs in Gram-negative pneumonia (21–23), the role of PAD4 in NET formation and the host response during bacterial pneumonia is currently unknown. We and others have previously shown that the common Gram-negative respiratory pathogen *K. pneumoniae* can induce NET formation in vitro (24, 25) and during pneumonia in vivo (22, 26). We, in this study, aimed to investigate the role of PAD4 in the formation of NETs, restriction of the infection, and local and systemic inflammatory and procoagulant responses during pneumonia caused by *K. pneumoniae*.

*Center for Experimental and Molecular Medicine, Academic Medical Center, University of Amsterdam, 1105 AZ Amsterdam, the Netherlands; †Electron Microscopy Center Amsterdam, Department of Medical Biology, Academic Medical Center, University of Amsterdam, 1105 AZ Amsterdam, the Netherlands; ‡Department of Pathology, Academic Medical Center, University of Amsterdam, 1105 AZ Amsterdam, the Netherlands; §Bioceros, 3584 CM Utrecht, the Netherlands; and ¶Division of Infectious Diseases, Academic Medical Center, University of Amsterdam, 1105 AZ Amsterdam, the Netherlands

ORCIDs: 0000-0002-6576-4787 (H.A.v.V.); 0000-0001-6392-3417 (N.N.v.d.W.); 0000-0001-8844-1326 (O.J.d.B.).

Received for publication March 1, 2018. Accepted for publication June 19, 2018.

T.A.M.C. was supported by a grant from the Landsteiner Foundation for Blood Transfusion Research (Grant 1351).

An abstract of this work was presented at the European Congress on Thrombosis and Haemostasis, September 28–30, 2016, The Hague, the Netherlands, and at the Congress of the International Society on Thrombosis and Haemostasis, July 8–13, 2017, Berlin, Germany.

Address correspondence and reprint requests to Dr. Theodora A.M. Claushuis, Center for Experimental and Molecular Medicine, Academic Medical Center, Meibergdreef 9, Room F0-117, 1105 AZ Amsterdam, the Netherlands. E-mail address: t.a.claushuis@amc.uva.nl

The online version of this article contains supplemental material.

Abbreviations used in this article: ALT, alanine aminotransferase; AST, aspartate aminotransferase; BALF, bronchoalveolar lavage fluid; cfDNA, cell-free DNA; CitH3, citrullinated H3; H3, histone 3; ICU, intensive care unit; LDH, lactate dehydrogenase; MPO, myeloperoxidase; NBL, nondirected bronchoalveolar lavage; NET, neutrophil extracellular trap; PAD4, peptidylarginine deiminase 4; TATc, thrombin–antithrombin complex; WT, wild-type.

Materials and Methods

Patients

Patients on the intensive care unit (ICU) with either pneumonia-derived sepsis or a noninfectious condition without lung pathology were subjected to a nondirected bronchoalveolar lavage (NBL) within 24 h of admission (27). NBL fluid was centrifuged for 15 min at 1500 × *g*, and supernatants were stored (27). Patients were included if they were older than 18 y and had at least two systemic inflammatory response syndrome criteria on the day of ICU admission (body temperature ≤36°C or ≥38°C, tachycardia >90 beats/min, tachypnea >20 beats/min or pCO_2 <4.3 kPA, and leukocyte count $<4 \times 10^9$ cells/l or $>12 \times 10^9$ cells/l) (28). The plausibility of infection was assessed using a four-point scale (ascending from none, possible, and probable to definite) as described in detail (29). Pneumosepsis was defined as the presence of pneumonia diagnosed within 24 h after ICU admission with a probable or definite likelihood, accompanied by at least one additional parameter as described in the 2001 International Sepsis Definitions Conference (30). Noninfectious ICU controls had an infection likelihood of none and a normal chest x-ray. The medical ethical committee of the Academic Medical Center in Amsterdam approved the conduction of the study (Institutional Review Board no. NL 34294.018.10) and written informed consent was obtained from all patients (or legal representative).

Animals

PAD4-deficient ($^{-/-}$) mice were generated by targeted deletion of *padi4*, the gene encoding PAD4, as described (11). $PAD4^{-/-}$ and $PAD4^{+/+}$ mice (on a C57BL/6 background) were bred and housed in the Animal Research Institute Amsterdam facility under standard care. All experiments were conducted with gender-matched mice between 8 and 12 wk of age. The Institutional Animal Care and Use Committee of the Academic Medical Center approved all experiments.

Experimental study design

Pneumonia was induced by intranasal inoculation with *K. pneumoniae* serotype 2 (43816; American Type Culture Collection, Rockville, MD; 10^4 CFUs in 50 μl of isotonic saline) (26). Mice were euthanized 12 or 42 h postinfection with *K. pneumoniae* (n = 8 per group); noninfected mice were sacrificed simultaneously (n = 4 per group). The t = 42 h time point was performed twice. Pneumonia was moreover induced by intranasal inoculation with *Pseudomonas aeruginosa* (strain PA01; 5×10^6 CFUs in 50 μl of isotonic saline), after which mice were euthanized at 6 or 24 h (31, 32). In a separate experiment, neutrophil-depleting anti-GR1 (clone RB6.8C5; rat IgG IgG2b, κ) or isotype control Ab anti-phytochrome (clone AFRC Mac 5.1; rat IgG IgG2b, κ) were administered i.p (33). Harvesting of samples, bacterial quantification, storage, and bronchoalveolar lavage were performed as described (26).

Electron microscopy

Total lungs of $PAD4^{+/+}$ and $PAD4^{-/-}$ mice infected for 42 h with *K. pneumoniae* were fixed in 0.1 M phosphate buffer with 4% paraformaldehyde and 1% glutaraldehyde immediately after sacrifice. Lungs were embedded using increasing gelatin concentrations up to 12%, and tissue slides were cut using a cryotome (Cryostar NX70, Thermo Fisher Scientific, Waltham, MA). Sections were stained for citrullinated H3 (CitH3) as described above. When an infected region was identified based on CitH3 staining, the remaining lung tissue was used for scanning electron microscopy. To improve scanning electron microscopy analysis, gelatin was first removed by washing the lung in phosphate buffer at 37°C followed by overnight fixation at room temperature. The sample was consequently dehydrated by washing steps with water and increasing concentrations of ethanol and, as a final step, hexamethyldisilazane (Sigma-Aldrich, Saint Louis, MO). After 24 h of drying, the sample was fixed to a holder using Conductive Carbon Cement (Electron Microscopy Sciences, Hatfield, PA) and gold coated using a Balzers SCD-040 (Oerlikon Balzers, Balzers, Liechtenstein). All images were made using a Zeiss Sigma-300 FE scanning electron microscope. Pictures of previously sectioned and CitH3-stained lungs were correlated to scanning electron microscopy images of the remaining lung surface using image navigation software (Zeiss, Oberkochen, Germany). This allowed scanning electron microscopy imaging of the tissue exactly at the location of CitH3-positive signal. Pictures were taking with a SE2 detector at 2 and 5 Kv with a working distance of 8.5 mm.

Assays

IL-6, IL-1β, and TNF-α were determined using cytometric beads array multiplex assay (BD Biosciences, San Jose, CA). CXCL1, CXCL2, and elastase were determined by ELISA (all R&D Systems, Minneapolis, MN) as well as thrombin–antithrombin complex (TATc) levels (Affinity Biologicals, Hamilton, Canada). D-dimer formation was determined by Western blot on lung homogenates by using a rabbit anti-mouse fibrinogen Ab (MyBioSource, San Diego, CA) at 180 kDa. Positive control for D-dimer was generated with murine recalcified citrated plasma activated with Innovin 1:1000 (Baxter, Utrecht, the Netherlands) in the presence of 2 μg/ml recombinant human tissue-type plasminogen activator (Actilyse; Boehringer Ingelheim) for 1 h at 37°C. Aspartate aminotransferase (AST), alanine aminotransferase (ALT), and lactate dehydrogenase (LDH) were measured using a c702 Roche Diagnostics analyzer (Roche Diagnostics, Almere, the Netherlands). Nucleosome levels were determined by ELISA as described (34). In brief, mAb CLB-ANA/60, which recognizes H3, was used as a capture Ab. Biotinylated CLB-ANA/58, which recognizes an epitope exposed on complexes of histone 2A, histone 2B, and dsDNA, in combination with poly-HRP, was used for detection. Cell-free DNA (cfDNA) was determined in plasma or bronchoalveolar lavage fluid (BALF); samples were diluted 50- to 100-fold with PBS containing 0.1% BSA and mixed with an equal volume of 1 μM SytoxGreen (Thermo Fisher Scientific). Fluorescence was immediately determined by a fluorescence microplate reader (Biotek, Winooski, VT). cfDNA was quantified using a DNA sample with a known concentration and background fluorescence of PBS with 0.1% BSA subtracted from all samples.

CitH3 and H3 Western blot

Levels of CitH3 and H3 in NBL and BALF were determined by Western blot. Samples were resolved by SDS-PAGE on 12% polyacrylamide gels under reducing conditions and proteins were transferred to PVDF membranes. Blots were blocked with 5% milk powder in Tris-buffered saline and 0.1% Tween (pH 7.4) for 2 h at room temperature, incubated with rabbit anti-CitH3 (1:1500, both anti-human and -mouse; Abcam, Cambridge, U.K.) or rabbit anti-H3 (1:1000, both anti-human and -mouse; Cell Signaling, Danvers, MA) overnight at 4°C, and subsequently incubated with anti-rabbit IgG-HRP (1:1000; Cell Signaling Technology, Leiden, the Netherlands) for 2 h at room temperature. Immunoreactive bands were visualized using an ImageQuant LAS 4000 (Fujifilm, Tokyo, Japan).

Ex vivo NET formation and stimulations

Neutrophils were isolated from the bone marrow of naive $PAD4^{+/+}$ and $PAD4^{-/-}$ mice using anti-mouse–Ly6G magnetic beads (Miltenyi Biotec, Bergisch Gladbach, Germany) in accordance with the manufacturer's instructions. Isolated mouse neutrophils were resuspended in PBS supplemented with 10 mM D-glucose at a concentration of 2×10^6 cells/ml, seeded onto poly-L-lysine–coated (Sigma-Aldrich) glass slides, and stimulated with 1 μg/ml LPS (from *K. pneumoniae*; Sigma-Aldrich), 10^7 CFUs of UV-radiated *K. pneumoniae*, or 100 nM PMA (Sigma-Aldrich) in the presence of 2 mM calcium for 3 h at 37°C and 5% CO_2. Samples were fixated with 4% paraformaldehyde (Electron Microscopy Sciences), washed with Perm/Wash buffer (BD Biosciences, San Diego, CA), and incubated with rabbit anti-myeloperoxidase (MPO) (Dako, Santa Clara, CA) and FITC-conjugated secondary Ab. DAPI (Thermo Fisher Scientific, Eugene, OR) was used to stain DNA. Images were obtained using an AxioVert fluorescence microscope (Zeiss) and a 20× objective lens and captured using AxioVision Rel. 4.8 software (Zeiss). Alternatively, NETs were incubated with citrated whole blood from $PAD4^{+/+}$ mice for 30 min at room temperature to assess platelet activation by flow cytometry (see below), or 10^3 CFUs of *Klebsiella* for 2 h to assess bacterial growth inhibition.

Flow cytometry

Platelet counts were measured in citrated whole blood by flow cytometry (FACSCalibur; Becton Dickinson, Franklin Lakes, NJ) using hamster anti-CD61 mAb (BioLegend, San Diego, CA). Platelet activation was determined by using rat anti-CD62 mAb (BD Biosciences) and anti-CD63 mAb (eBioscience, San Diego, CA) in combination with an appropriate IgG control.

Pathology and immunohistochemistry

The paraffin-embedded left lung and liver were cut into 4-μm sections and stained with H&E. Slides were coded and scored by a pathologist blinded for group identity as described (25). Distinct parameters were scored in the range of 0 (absent) to 4 (most severe). For the lung, these were as follows: percentage of lung infiltrated, interstitial inflammation, endothelialitis, bronchitis, edema, pleuritis, bleeding, and presence of thrombi; the scores of all parameters were added for the total histopathological score, with a maximum score of 32 (35). For the liver inflammation, necrosis and presence of thrombi were scored, with a maximum score of 12 (25).

Paraffin sections were stained for the presence of CitH3 with a rabbit polyclonal Ab directed against CitH3 (1:4000; Abcam) (36) and anti-rabbit

IgG-HRP (Immunologic, Duiven, the Netherlands) using NovaRED (Vector Laboratories, Burlingame, CA) and counterstained with hematoxylin.

Additionally, CitH3-MPO double stainings were done as described (37, 38). In short, neutrophils were visualized using a rabbit polyclonal anti-MPO Ab (1:2500; Dako, Carpinteria, CA), followed by anti-rabbit IgG-HRP and NovaRED. Then, sections were digitized in a slide scanner, destained, and restained with anti-CitH3 Ab and NovaRED. After scanning these slides, (false-color) images were created using ImageJ (U.S. National Institutes of Health, Bethesda, MD). To determine neutrophil influx in the lung, sections were stained with anti-mouse Ly6G mAb (BD Pharmingen, San Diego, CA) as previously described (26). Fibrinogen staining on lung sections was performed as previously described (39) using a goat anti-mouse fibrinogen Ab (Accurate Chemical & Scientific, Westbury, NY). Slides were scanned using an Olympus dotSlide scanner (Olympus, Tokyo, Japan) to generate TIFF images of the full tissue section. CitH3, Ly-6G, and fibrinogen positivity was measured using ImageJ; the amount of positivity was expressed as percentage of the total lung surface area (26, 39).

Statistical analysis

Data are expressed as scatter plots with horizontal lines representing medians. For animal experiments, comparisons between groups were first performed using a one-way ANOVA on ranks. When significant differences were present, groups at individual time points were tested using the Mann–Whitney *U* test. For analysis of ICU patients, the Mann–Whitney *U* test was performed to analyze the difference between the two groups. Analyses were done using GraphPad Prism 5.01 (GraphPad Software, San Diego, CA). The p values <0.05 were considered statistically significant.

Table I. Baseline characteristics of ICU patients

	ICU Controls	Pneumosepsis
Patients admissions, *n* (%)	4	6
Gender male, *n* (%)	3 (75%)	5 (83.3%)
Age (y), mean (SD)	48 (14.1)	59 (7.5)
Diagnosis		
Intracranial hemorrhage	1 (25%)	
Spinal cord surgery	1 (25%)	
Upper GI bleeding	1 (25%)	
Abdominal trauma	1 (25%)	
Hospital-acquired pneumonia		2 (33.3%)
Community-acquired pneumonia		4 (66.7%)
Causative pathogen		
Aspergilles species		1 (16.7%)
Streptococcus pneumoniae		3 (50%)
Unknown		2 (33.3%)
APACHE IV score, median (IQR)	70.8 (61.3–75.5)	68.5 (63–74)
Mechanical ventilation, *n* (%)	4 (100%)	6 (100%)
Shock, *n* (%)	1 (25%)	2 (33.3%)
28-d mortality, *n* (%)	2 (50%)	4 (66.7)

APACHE, Acute Physiology and Chronic Health Evaluation; GI, gastrointestinal; IQR, interquartile range.

Results

Evidence of PAD4 activation in BALF of patients with pneumosepsis

To obtain insight into the activation of PAD4 in the airways of patients with pneumonia, we measured CitH3 in NBL harvested from ICU patients with pneumosepsis and ICU control patients without infection or lung pathology (Table I) by Western blotting. Although none of the four ICU control patients showed a signal of CitH3 in their lavage fluid, five of six pneumonia patients had detectable CitH3 (Fig. 1A, upper panel, and uncropped images in Supplemental Fig. 1). Increased levels of CitH3 might be related to NET formation; therefore, we assessed other markers of NET formation. H3 was also exclusively detected in lavage fluid of pneumosepsis patients (Fig. 1A, lower panel), and levels of cfDNA, nucleosomes, and the nucleosomes/cfDNA ratio in lavage fluid tended to be higher in patients with pneumosepsis than in ICU controls (Fig. 1B–D). These data suggest that several NET-derived products, including CitH3, cfDNA, and nucleosomes, are present in the airways of ICU patients with pneumonia.

K. pneumoniae *induces increased neutrophil-derived CitH3*

To further assess PAD4 activation during pneumonia, we infected PAD4$^{+/+}$ and PAD4$^{-/-}$ mice with the common human respiratory pathogen *K. pneumoniae* via the airways and stained lung sections for CitH3 (36). *K. pneumoniae* infection induced citrullination of H3 in the lung, primarily at the site of infiltration of immune cells (Fig. 2A, CitH3 stained red). PAD4$^{-/-}$ mice did not show CitH3-positive areas in their lungs, and also not at sites of immune cell infiltration (Fig. 2A, 2B). To assess whether areas of H3 citrullination colocalized with neutrophils and other NET components (11), we costained with neutrophil marker MPO. CitH3 colocalized with MPO in lung tissue slides of PAD4$^{+/+}$ mice infected with *Klebsiella*, suggesting CitH3 was neutrophil-derived. In PAD4$^{-/-}$ mice, lung sections only stained positive for MPO (Fig. 2B). Neutrophil influx in the lung (as determined by Ly6G staining) was not impaired in PAD4$^{-/-}$ mice, which even had slightly more neutrophils present in the lung 12 h postinfection (Supplemental Fig. 2). To ensure neutrophils were the major source of CitH3 in the lungs during pneumonia, we depleted wild-type (WT) mice of neutrophils prior to infection with *Klebsiella* using an anti-GR1 Ab (33). Neutrophil depletion was confirmed in peripheral blood and was associated with an enhanced bacterial growth in the lungs when compared with mice treated with a nondepleting control Ab (Supplemental Fig. 2). Lungs of neutrophil-depleted mice did not stain positive for CitH3 (Fig. 2C). These data indicate that *K. pneumoniae*–induced pneumonia induces neutrophil-derived CitH3. In contrast to findings in the lung, we found no evidence for H3 citrullination in the livers of PAD4$^{+/+}$ (or PAD4$^{-/-}$) mice (Supplemental Fig. 2).

Visualization of CitH3-positive areas during K. pneumoniae*–induced pneumonia by electron microscopy*

To assess whether CitH3 correlated with NET formation, we used scanning electron microscopy to visualize the lungs of PAD4$^{+/+}$ mice infected with *K. pneumoniae*. This was done by combining light microscopy and electron microscopy. Lung sections were first cut and stained for CitH3, and subsequently, the remaining lung tissue was visualized with scanning electron microscopy and images of CitH3 staining were matched to scanning electron microscopy images using navigation software to allow for localization of CitH3-positive sites. In areas of CitH3-positive staining (arrow in Fig. 3A), bronchi were frequently obstructed and *Klebsiella* bacteria were abundantly seen (Fig. 3B–D). Within and at the periphery of these obstructed bronchi, *Klebsiella* bacteria were frequently seen surrounded and captured by threadlike strands, likely NETs (Fig. 3D).

PAD4-independent NETosis is present during K. pneumoniae*–induced pneumonia*

To assess whether PAD4 inhibition reduced NET formation, the lungs of infected PAD4$^{-/-}$ mice were also assessed by scanning electron microscopy. To our surprise, similar NET-like structures were seen in PAD4$^{-/-}$ mice (Fig. 3E, 3F) abundantly surrounding *Klebsiella* bacteria at sites of immune infiltration. No ultrastructural differences between strands capturing bacteria in WT versus PAD4$^{-/-}$ mice were detected. Moreover, although CitH3 was not detectable in BALF of PAD4$^{-/-}$ mice (Fig. 4A, 4B and uncropped images in Supplemental Fig. 1), H3 levels were not significantly

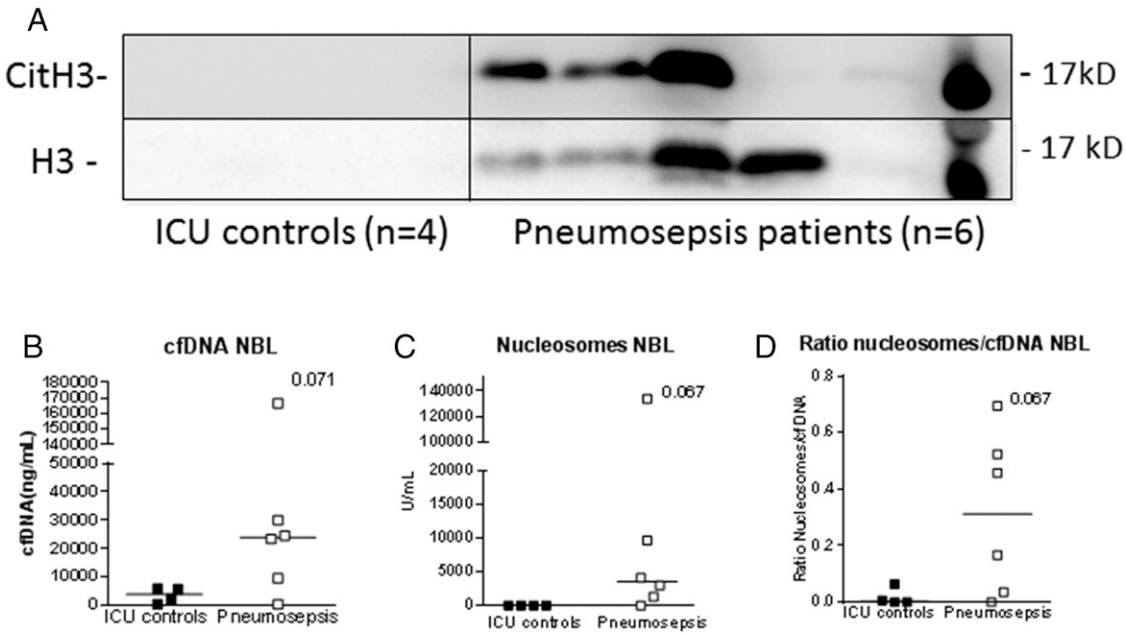

FIGURE 1. CitH3, cfDNA, and nucleosome concentrations in the airways of critically ill patients with pneumosepsis or noninfectious nonpulmonary disease. (**A** and **B**) ICU patients without infection or lung disease ($n = 4$) and pneumosepsis patients ($n = 6$) were subjected to an NBL within 24 h after ICU admission. (A) CitH3 (upper panel) and H3 (lower panel) were assessed by Western blotting. (B) cfDNA and (**C**) nucleosome levels in NBL. (**D**) Ratio nucleosome/cfDNA. Data are presented as scatter dot plots and horizontal lines represent median. Groups were compared using Mann–Whitney *U* test as data were not normally distributed.

different in both mouse strains (Fig. 4A, 4B). We also determined cfDNA, nucleosome, MPO, and elastase levels in BALF and plasma harvested 42 h postinfection. $PAD4^{-/-}$ mice showed slightly lower cfDNA levels in BALF (Fig. 4C, $p < 0.05$ versus $PAD4^{+/+}$ mice); however, nucleosome, MPO, and elastase levels were similar between groups (Fig. 4D–F). $PAD4^{-/-}$ and $PAD4^{+/+}$ mice had similar numbers of neutrophils in BALF (64.1 [60.2] versus 80.9 [56.5] $\times$ 10^4/ml [median with interquartile range], respectively). *Klebsiella* pneumosepsis resulted in increased plasma concentrations of cfDNA, nucleosomes, MPO, and elastase; none of these markers were different between $PAD4^{-/-}$ and $PAD4^{+/+}$ mice (Fig. 4G–J). Together, these results suggest that NETosis can occur by a PAD4-independent mechanism during *K. pneumoniae*–induced pneumosepsis.

NET formation can occur in the absence of PAD4

As in vivo data suggested that NETs can still be formed in the absence of PAD4, neutrophils were isolated from $PAD4^{-/-}$ and $PAD4^{+/+}$ mice and stimulated to induce NETs. $PAD4^{+/+}$ neutrophils stimulated with PMA, LPS, or UV-radiated *Klebsiella* produced NET-like structures with positive staining for both DNA and MPO (Fig. 5). In line with findings in vivo, these structures were also seen upon stimulation of $PAD4^{-/-}$ neutrophils (Fig. 5, with overview photos in Supplemental Fig. 3). These data also indicate that ex vivo, NET formation induced by *K. pneumoniae* or bacterial components can still occur in the absence of PAD4.

PAD4 deficiency does not affect bacterial growth in K. pneumoniae*–induced pneumonia and sepsis*

To study a possible role of PAD4 in limiting bacterial growth during *K. pneumoniae*–induced pneumonia and sepsis, we determined bacterial numbers at the primary site of infection (lungs) and distant body sites (blood, spleen, and liver) in infected $PAD4^{+/+}$ and $PAD4^{-/-}$ mice. At 12 h, when bacteria had not yet disseminated, $PAD4^{-/-}$ mice had minimally increased bacterial loads in the lung, as compared with $PAD4^{+/+}$ mice (Fig. 6A, $p < 0.05$). At 42 h, however, $PAD4^{+/+}$ and $PAD4^{-/-}$ mice had similar bacterial loads in the lungs and distant organs (Fig. 6A–D). Moreover, NETs generated from $PAD4^{-/-}$ and $PAD4^{+/+}$ neutrophils showed similar growth inhibition of *Klebsiella* ex vivo (Fig. 6E).

We additionally used a different model of Gram-negative pneumonia, infection with *P. aeruginosa*, to assess the role of PAD4 on host defense. This infection results in an acute infection that is subsequently cleared (31, 32). Also using this model of Gram-negative infection, $PAD4^{+/+}$ and $PAD4^{-/-}$ mice showed comparable bacterial loads (Supplemental Fig. 2).

PAD4 deficiency does not impact lung inflammation during K. pneumoniae*–induced pneumonia*

PAD4 can directly influence cytokine expression and thereby modulate lung inflammation during pneumonia (7, 8). Pneumosepsis resulted in strong increases in lung cytokine (TNF-α, IL-1β, and IL-6) and chemokine (CXCL1 and CXCL2) levels; however, no differences were detected between $PAD4^{+/+}$ and $PAD4^{-/-}$ mice (Fig. 7A–E). We also scored the extent of lung inflammation, making use of a scoring system that incorporates the main histological features of pneumonia (26). Infection resulted in lung pathology consistent with pneumonia, but no differences were found between $PAD4^{+/+}$ and $PAD4^{-/-}$ mice (Fig. 7F, 7G). These data indicate that PAD4 does not influence the local inflammatory response during *Klebsiella* pneumonia.

PAD4 deficiency does not influence sepsis-induced distant organ damage

PAD4 mediated NETs have been implicated in liver damage (19, 40). The model of *Klebsiella* pneumosepsis is associated with hepatocellular injury, as reflected by elevated plasma levels of AST and ALT (26). Consistently, liver tissue showed areas of inflammation and necrosis, which, however, were equally present in both mouse strains at 42 h postinfection (Fig. 7H, 7I). Likewise,

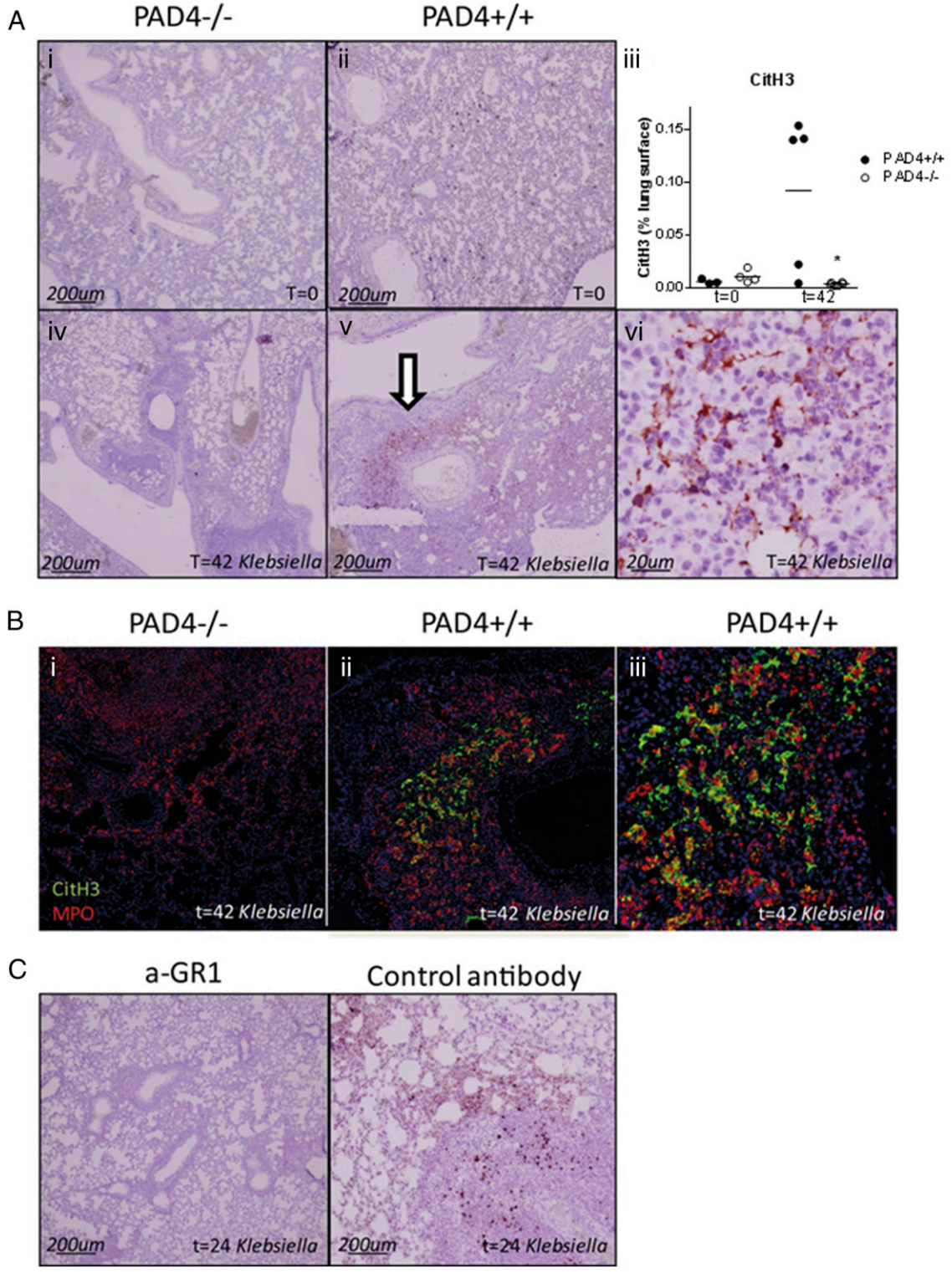

FIGURE 2. CitH3 is induced in the lung during pneumonia, mainly at sites of immune cell infiltration, and absent in PAD4$^{-/-}$ mice. (**A**) CitH3 staining of lung sections (original magnification ×40) of (**Ai** and **Aii**) naive and (**Aiv**–**Avi**) *Klebsiella*-infected (t = 42 h) PAD4$^{+/+}$ or PAD4$^{-/-}$ mice. (**Aiii**) Quantification of CitH3 staining expressed as scatter dot plot of four to six mice per group. Horizontal lines represent median. *$p < 0.05$. (Avi) Increased magnification (original magnification ×400) of CitH3 staining during infection in PAD4$^{+/+}$ mice. Arrow indicates CitH3-positive area identified with scanning electron microscopy in (**B**). (B) Digital overlay of double staining of CitH3 and MPO in lung sections (original magnification ×100) of infected PAD4$^{+/+}$ and PAD4$^{-/-}$ mice 42 h postinfection with *Klebsiella*. CitH3 in green, MPO in red. (Biii) Increased magnification of double staining of CitH3 and MPO in lung sections of infected PAD4$^{+/+}$ mice. (**C**) CitH3 staining of lung sections (original magnification ×100) of IgG control–treated or anti-GR1 (aGR1)–treated (neutropenic) mice 24 h postinfection with *Klebsiella*.

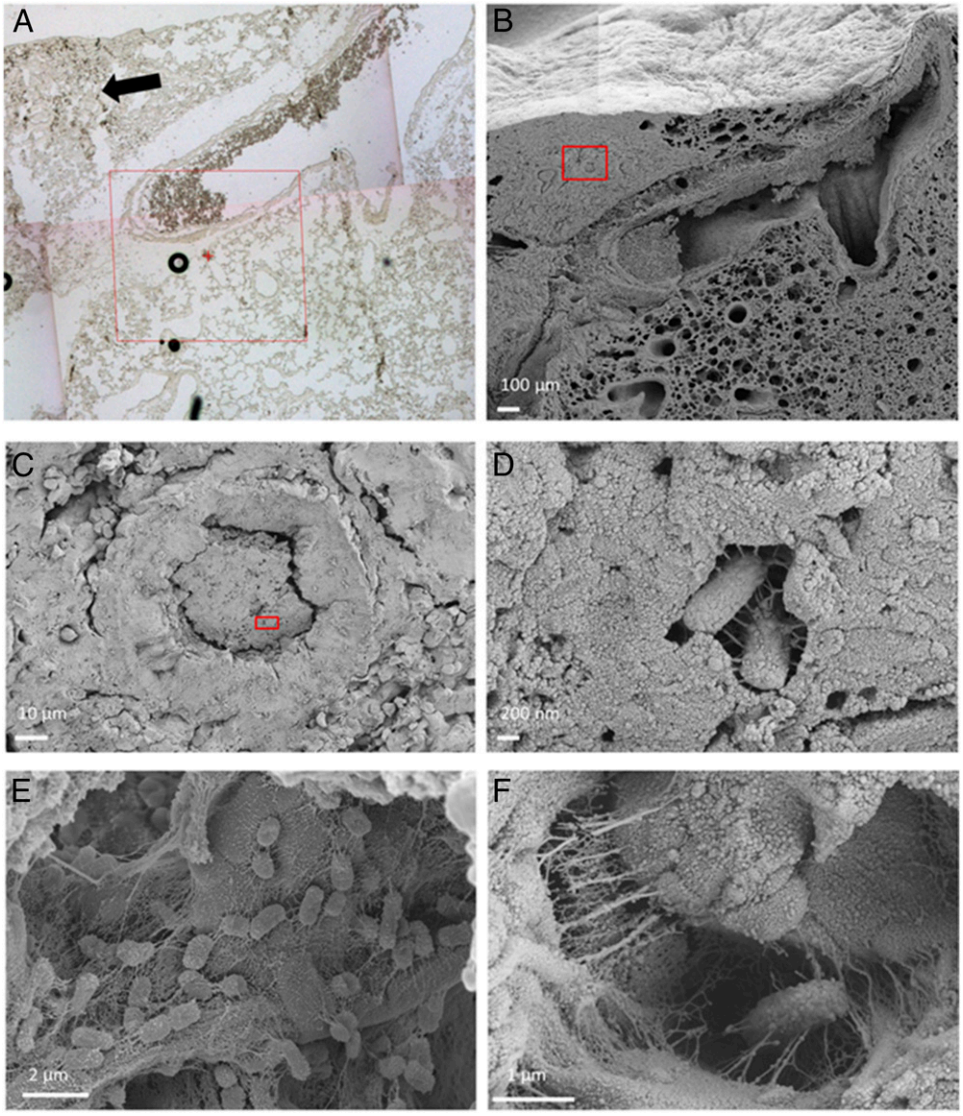

FIGURE 3. Scanning electron microscopy visualization of NET-like structures in the lung during pneumosepsis. (**A**) CitH3 staining of lung tissue harvested 42 h after *Klebsiella* infection of PAD4$^{+/+}$ mice; arrow indicates where CitH3 stained positive during staining. Original magnification ×40. (**B**–**D**) Areas of CitH3-positive signal visualized with scanning electron microscopy. (B) Obstructed lung bronchus with infiltrate; box indicates area shown enlarged in (C). (C) Higher magnification of obstructed lung bronchus; box indicates area shown enlarged in (D). (D) Higher magnification of obstructed lung bronchus showing *Klebsiella* captured within, surrounded by threadlike structures. (**E** and **F**) Scanning electron microscopy images of PAD4$^{-/-}$ mice, 42 h after *Klebsiella* infection, also showing *Klebsiella* surrounded by threadlike structures.

plasma concentrations of AST and ALT were equally elevated in PAD4$^{-/-}$ and PAD4$^{+/+}$ mice at 42 h postinfection (Fig. 7J, 7K). As a general marker of organ damage, we measured plasma LDH, which was similarly increased in PAD4$^{-/-}$ and PAD4$^{+/+}$ mice during *Klebsiella* pneumosepsis (Fig. 7L). These data indicate that PAD4 deficiency does not influence distant organ injury during pneumosepsis.

Influence of PAD4 deficiency on platelet activation and activation of coagulation

NET components are potent activators of platelets and coagulation [e.g., histones activate platelets via TLRs 2/4 (41) and cfDNA activates the intrinsic pathway of coagulation (41)]. We therefore investigated the contribution of PAD4 to platelet activation during pneumonia-derived sepsis. *Klebsiella* pneumosepsis was associated with platelet activation, as reflected by enhanced P-selectin and CD63 expression on circulating platelets; this was reduced in PAD4$^{-/-}$ mice, especially at 42 h postinfection (Supplemental Fig. 4). PAD4 deficiency, however, did not seem to mitigate sepsis-induced thrombocytopenia (Supplemental Fig. 4).

To further assess how PAD4 influences platelet activation, we incubated whole blood from naive PAD4$^{+/+}$ mice with (PMA-induced) NETs from either PAD4$^{-/-}$ or PAD4$^{+/+}$ mice. Although NETs induced platelet activation compared with unstimulated neutrophils, no differences were found between the effects of NETs from PAD4$^{-/-}$ or PAD4$^{+/+}$ mice (Supplemental Fig. 4).

To investigate the role of PAD4 in activation of coagulation, we assessed fibrin deposition and D-dimer formation in lungs and TATc levels in plasma and lungs postinfection with *Klebsiella*. Infection with *Klebsiella* resulted in activation of coagulation in lung and plasma (Supplemental Figs. 1, 4). However, there were no significant differences in any of the coagulation readouts between groups (Supplemental Figs. 1, 4), apart from lower TATc levels at baseline in the lungs of PAD4$^{-/-}$ mice (Supplemental Fig. 4). These results indicate that although PAD4 deficiency reduces platelet activation, it does not appear to affect thrombocytopenia nor activation of coagulation during *K. pneumoniae*. Previous investigations on the role of PAD4 on NET formation have reported partially conflicting results. Inhibition of PAD4 by genetic depletion or Cl-amidine–reduced PMA (42) or LPS (11, 43, 44) induced NET formation by murine neutrophils; however, NET formation by human neutrophils, induced by multiple stimuli including PMA and bacteria, was unaffected by PAD4 inhibition (18).

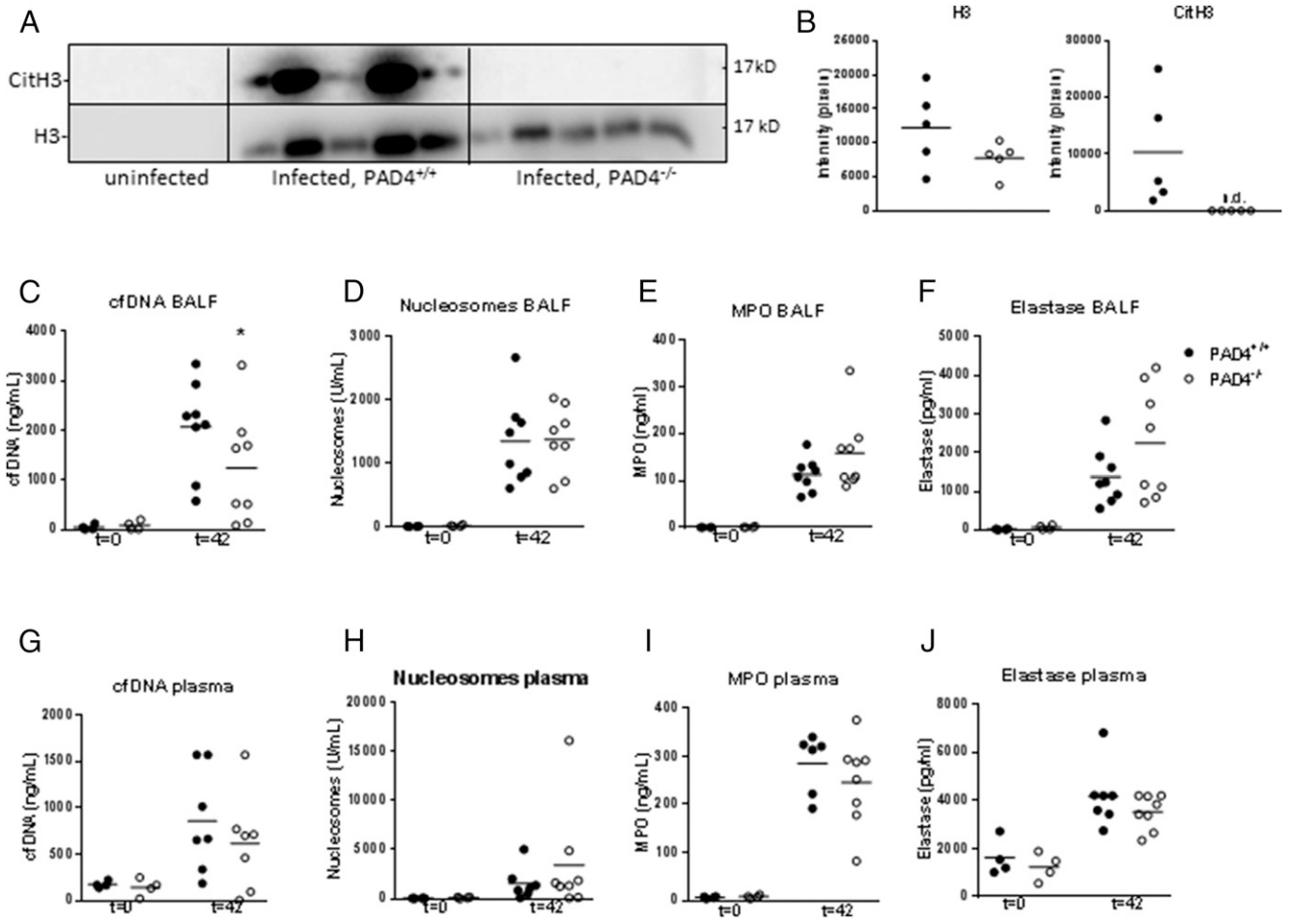

FIGURE 4. Markers of NET formation in lung and plasma during pneumosepsis. (**A**–**J**) PAD4$^{+/+}$ and PAD4$^{-/-}$ mice were euthanized before or 42 h postinfection with *K. pneumoniae* via the airways. (A) Western blot of CitH3 and H3 in BALF. (B) Quantification of Western blot. (C) cfDNA, (D) nucleosome, (E) MPO, and (F) elastase levels in BALF. (G) cfDNA, (H) nucleosome, (I) MPO, and (J) elastase levels in plasma. Data are presented as scatter dot plots of eight mice per group for infected mice and four mice per group for uninfected mice. Horizontal lines represent medians. Western blot shows comparison of five versus five mice. *$p < 0.05$ versus PAD4$^{+/+}$ mice. n.d., not detectable.

Discussion

PAD4 has been implicated as an important regulator of NET formation by mediating chromatin decondensation through hypercitrullination of H3 (10). However, other mechanisms can contribute to the release of NETs and controversy remains about the relative importance of PAD4 in NETosis (15, 16, 18, 45, 46). In this study, we show that although PAD4 is activated in the airways during human and murine pneumosepsis, NET formation can still occur independently of PAD4, and PAD4 has only a modest, if any, effect on other host responses implicated in sepsis pathogenesis in mice with pneumonia-derived sepsis caused by the common human pathogen *K. pneumoniae*.

Previous studies have shown NET components in plasma of sepsis patients or increased NET release by isolated neutrophils ex vivo (47, 48). In this study, we show that ICU patients with pneumonia had detectable CitH3 in their airways, together with high levels of cfDNA and nucleosomes. Of note, ICU patients without lung infection or pathology also had high cfDNA and nucleosome concentrations in NBL in the absence of detectable CitH3 (or H3), suggesting that either citrullination of H3 is not required for NETosis or that cfDNA and nucleosomes are not or are only partially derived from NETs. We combined these observational data in patients with investigations in an established model of Gram-negative pneumonia-derived sepsis by *K. pneumoniae* to show that CitH3 in the lungs originates from infiltrating neutrophils and is generated by a PAD4-dependent mechanism. By carefully matching scanning electron microscopy images with (neutrophil-derived) CitH3-positive areas in light microscopy, we visualized NET-like structures surrounding *Klebsiella* bacteria in infiltrated lung tissues, which is in accordance with a previous study (22). Remarkably, however, PAD4$^{-/-}$ mice had similar NET-like structures surrounding bacteria at sites of immune cell infiltration. Using electron microscopy, we found that not all bacteria were captured in these strands and the strands varied in thickness from 5 to 50 nm and sometimes branched into different directions. This suggests that the threadlike structures are not fibrin, which can vary in tissues from 50 to 400 nm. It is moreover not likely that these strands are mucus, as mucus shows a denser network with numerous branching when assessed with scanning electron microscopy (49). We cannot exclude that part of these structures are in fact of bacterial origin, as there is increasing evidence for dynamic tubular sheaths formed by the Type VI secretion system of *K. pneumoniae* (50, 51). These structures are however not well described in lung tissues and, as large regions, are covered with fibrils of various sizes, branching off into different directions, we assume that most of the threadlike strands are NETs. Moreover, other parameters associated with NET formation were not or were only modestly influenced by PAD4

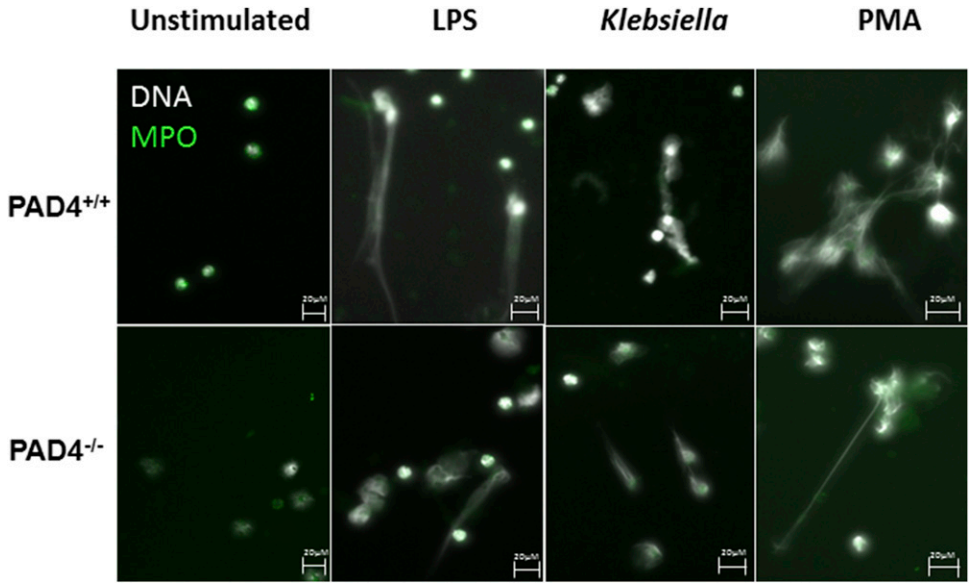

FIGURE 5. Ex vivo NET formation does not rely on PAD4. PAD4$^{+/+}$ and PAD4$^{-/-}$ neutrophils were stimulated with medium control, LPS, PMA, or UV-radiated *Klebsiella* for 3 h. NETs were visualized with immunofluorescence of MPO (in green) or DNA (DAPI staining in white).

deficiency, with reduced cfDNA in the BALF of PAD4$^{-/-}$ mice during *Klebsiella* pneumosepsis when compared with WT mice but no differences in plasma cfDNA levels or nucleosome, MPO, or elastase levels in BALF or plasma. Furthermore, stimulation of PAD4$^{-/-}$ neutrophils with various ligands, including LPS and *Klebsiella*, resulted in NET formation that was indistinguishable from the response of PAD4$^{+/+}$ neutrophils. Together, these data suggest NETosis during *K. pneumoniae*–induced pneumonia occurs through a PAD4-independent mechanism.

Previous investigations on the role of PAD4 on NET formation have reported partially conflicting results. Inhibition of PAD4 by genetic depletion or Cl-amidine–reduced PMA (42) or LPS (11, 43, 44) induced NET formation by murine neutrophils; however, NET formation by human neutrophils, induced by multiple stimuli, including PMA and bacteria, was unaffected by PAD4 inhibition (18). We found no effect of PAD4 elimination on ex vivo NET formation by mouse neutrophils induced by PMA, LPS, or *Klebsiella*. Differences between our findings and those of others could in part be explained by PAD4-independent effects of Cl-amidine (52, 53) that might influence NET release. Alternatively, as PAD4$^{-/-}$ mice did show reduced in vitro NET formation in other studies (11, 44), differences in methods for inducing NETosis might play a more crucial role. These differences include source of LPS, type of neutrophil isolation (EasySep Mouse Neutrophil Enrichment and density gradients versus Ly6G magnetic beads), or time (4 versus 3 h) and method of stimulation.

Besides PAD4, other mechanisms can contribute to NETosis, including elastase, MPO, production of reactive oxygen species, autophagy, and activation of p38 MAPK and Raf–MEK–ERK signaling pathways (18, 22, 45, 46, 54–57). It appears that these different pathways are not absolutely required for NET formation in general. For instance, *Straphylococcus aureus* can induce NETosis in human neutrophils independent of NADPH oxidase (58). In mice, neutrophil elastase was not important for NET formation during murine venous thrombosis in vivo or upon stimulation with noninfectious stimuli in vitro, whereas PAD4 was (59). In contrast, elastase-deficient mice were unable to form NETs in a pneumonia model that made use of a different *Klebsiella* strain used in this study (22), whereas our current data indicate no role for PAD4 in this study. In fulminant sepsis models induced by *S. aureus*, *Escherichia coli*, or LPS, PAD4 deficiency reduced NET release in the liver (12, 40). In accordance, a recent study in human neutrophils clearly showed that different stimuli rely on different upstream pathways to induce NETosis (18). Of note, we could not detect CitH3 in liver tissue, which is in agreement with an earlier study by our group that showed that this model of *Klebsiella* sepsis is not associated with NET formation in liver (26).

Studies investigating the role of PAD4 in infection have used either PAD4$^{-/-}$ mice or the pan-PAD inhibitor Cl-amidine (60). PAD4$^{-/-}$ mice were more susceptible to skin infection caused by a mutant group A *Streptococcus* lacking an extracellular DNAse but not when infected by WT group A *Streptococcus* (11). PAD4 deficiency influenced neither host defense during abdominal sepsis induced by cecal ligation and puncture (20) nor influenza infection (61). Other studies using PAD4$^{-/-}$ mice did find reduced coagulation (19) and liver damage (19, 40) after injection of *S. aureus* or *E. coli* but did not report on antibacterial defense. Several studies found beneficial effects of Cl-amidine treatment on mortality after cecal ligation and puncture (62–64); the difference with results obtained with PAD4$^{-/-}$ mice may be related to aspecific PAD inhibition by Cl-amidine (52, 53). Overall, current data do not support an important direct role for PAD4 in host defense during sepsis.

PAD4 has been reported to influence inflammation by modulating cytokine expression (7, 8). During pneumosepsis, PAD4 deficiency did not modify cytokine levels, suggesting that in this setting the influence of PAD4 on cytokine production is inferior to other regulators of cytokine production.

PAD4 inhibition had a small but significant effect on platelet activation during pneumosepsis. To further investigate this, we assessed whether PAD4-mediated NET formation influences platelet activation by incubating blood from naive PAD4$^{+/+}$ mice with NETs generated from PAD4$^{-/-}$ or PAD4$^{+/+}$ neutrophils. Platelet activation was similar between groups, indicating that

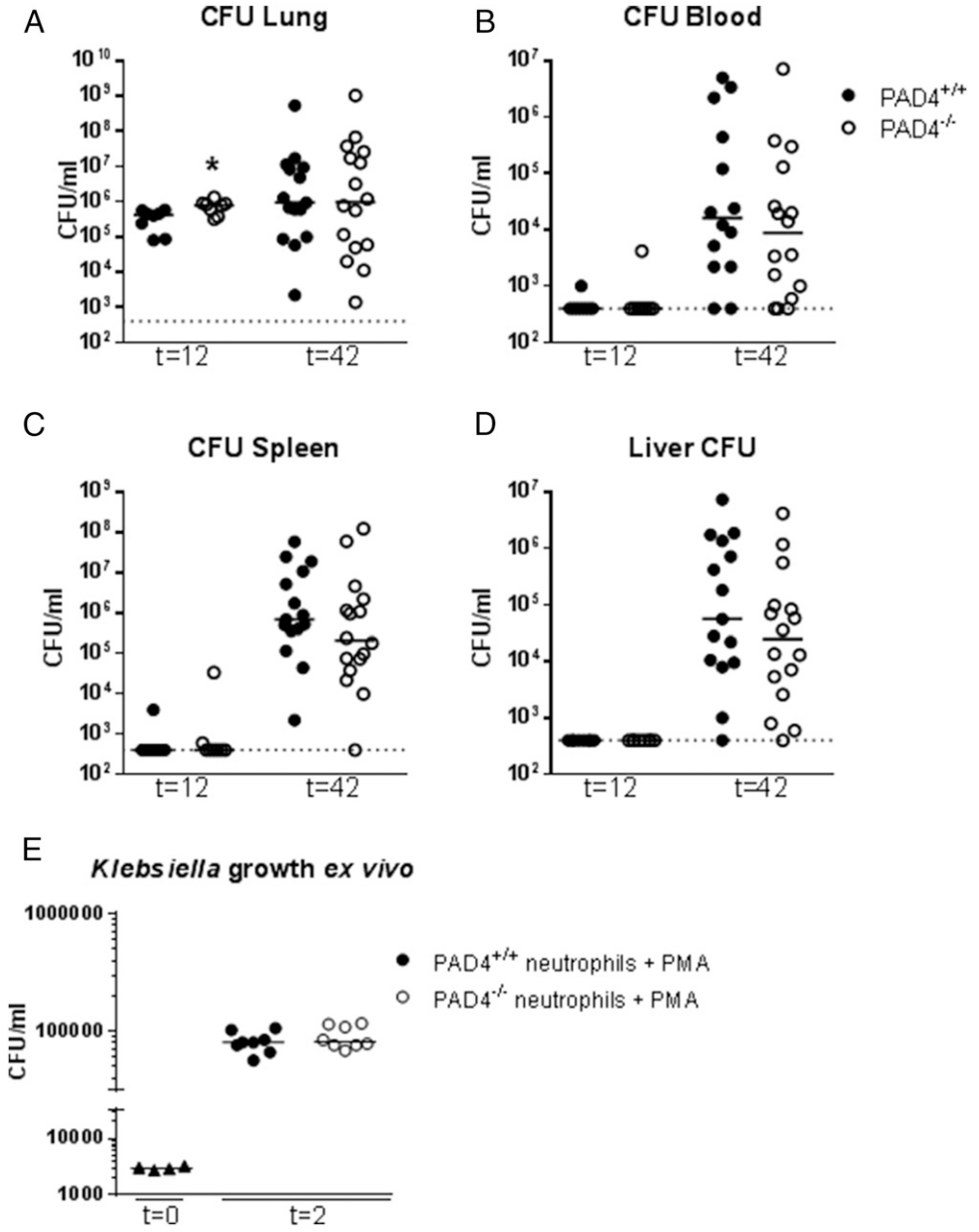

FIGURE 6. PAD4 deficiency does not strongly impact bacterial growth or dissemination during pneumosepsis. (**A**–**D**) PAD4$^{+/+}$ and PAD4$^{-/-}$ mice were infected with *K. pneumoniae* via the airways and euthanized at 12 or 42 h. Bacterial counts were determined in the lungs (A), blood (B), liver (C) and spleen (D). (**E**) PAD4$^{+/+}$ and PAD4$^{-/-}$ neutrophils were isolated from bone marrow and NETs were induced with PMA, after which *Klebsiella* was added and growth was assessed after 2 h. Data are presented as scatter dot plots of eight mice or replicates per group for ex vivo and $t = 12$ and 16 mice per group for $t = 42$ (pooled data of two experiments using eight mice per group). Horizontal lines represent medians. $*p < 0.05$.

the quality of NETs derived from PAD4$^{+/+}$ and PAD4$^{-/-}$ neutrophils is similar with regard to the capacity to activate platelets. Possibly, citrullinated histones are capable of inducing platelet activation.

The use of viable bacteria in our model of *Klebsiella*-induced pneumonia and sepsis can result in increased variation within groups. This is especially seen at later a time point, when the interaction between bacterial growth and the immune response can differ for each mouse. Although this variation can hamper interpretation of the results, this model has extensively been used to show significant differences between groups despite variation (26, 65, 66). Moreover, we have quantified the effect of PAD4 on bacterial loads in two separate ($t = 42$) pneumosepsis experiments, resulting in a larger sample size and enabling us to draw conclusions regarding the effect of PAD4 on host defense. Moreover, additional experiments using a different Gram-negative bacterium, *P. aeruginosa*, also showed no effect of PAD4 on host defense.

PAD4 has been implicated as a mediator of both host defense and collateral tissue damage during severe infection. Pneumonia is the most frequent cause of sepsis. We used a model of pneumonia-derived sepsis with a common human pathogen that is associated with a gradually growing bacterial load eventually resulting in dissemination (unlike fulminant sepsis models), allowing analyses of both early protective innate immunity and late detrimental host responses. We found evidence for PAD4 activation during human and murine pneumosepsis. NETs could, however, still be formed despite PAD4 deficiency, and PAD4 did not influence host responses in infected mice. Our data argue against a role for PAD4 in the pathogenesis of sepsis.

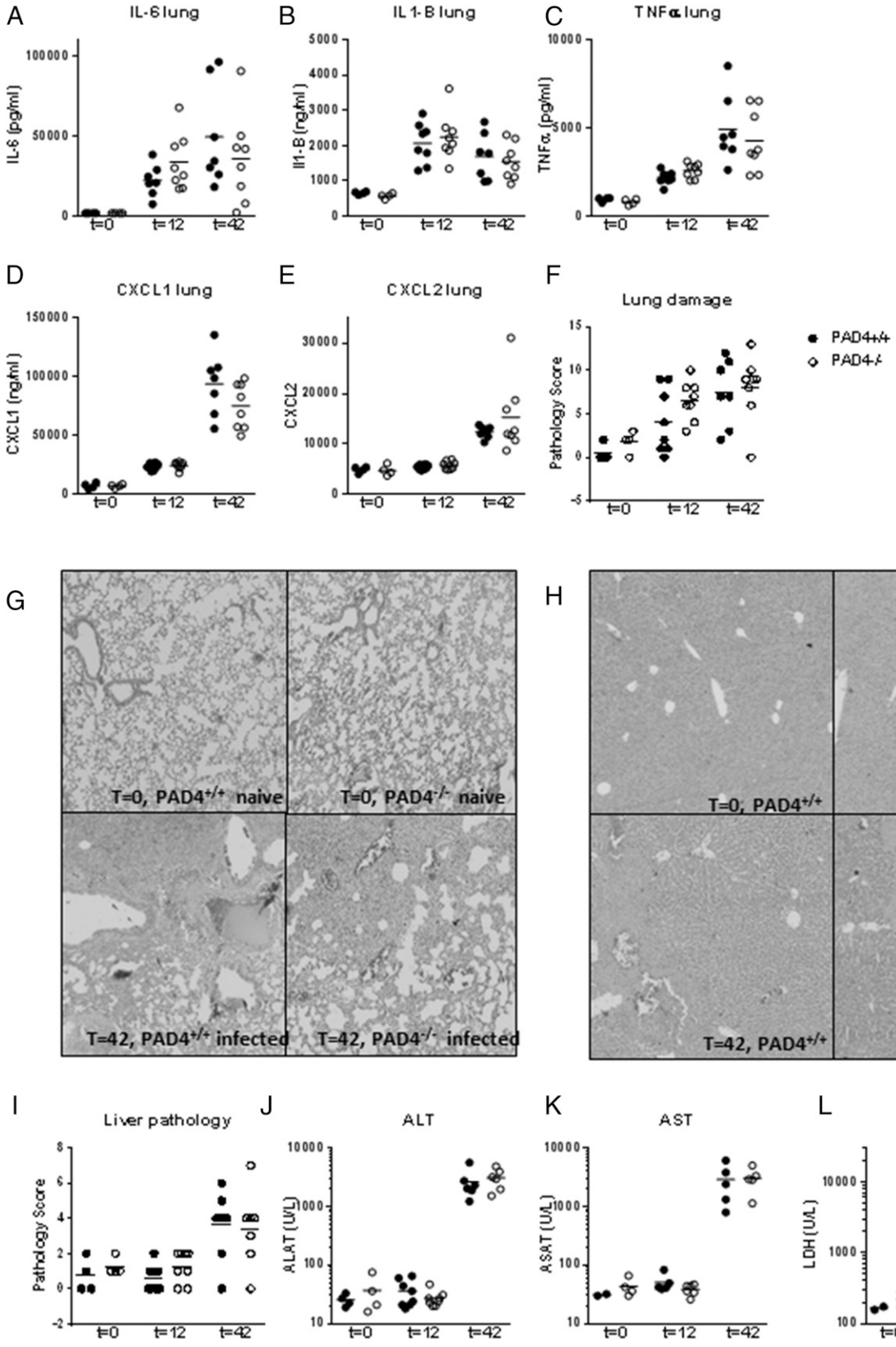

FIGURE 7. PAD4$^{-/-}$ mice have unaltered lung inflammation and distant organ damage during pneumosepsis. (**A**–**G**) PAD4$^{+/+}$ and PAD4$^{-/-}$ mice were infected with *K. pneumoniae* via the airways. (A) IL-6, (B) IL-1β, (C) TNF-α, (D) CXCL1, and (E) CXCL2 levels in lung homogenates. (F) Total lung histopathology scores. (G) Representative photographs of H&E-stained lung sections. (**H**) Representative photographs of H&E-stained liver sections. Original magnification ×40. (**I**) Total liver histopathology scores. Plasma levels of AST (**J**) and ALT (**K**) (markers for hepatocellular injury). (**L**) Plasma levels of LDH (general cell injury marker). Data are presented as scatter dot plots of eight mice per group for infected mice and four mice per group of uninfected mice. Horizontal lines represent medians. Differences between PAD4$^{+/+}$ and PAD4$^{-/-}$ mice were not statistically significant.

Acknowledgments

We thank M. ten Brink, J. Daalhuisen, and G. Krebbers for technical assistance and B. Cortjens for technical assistance with Fig. 2A–F. We thank Prof. Zychlinsky (Max Planck Institute for Infection Biology, Berlin, Germany) for sending the PAD4$^{-/-}$ mice, which originally were received from Prof. D. Wagner (Harvard, Cambridge, MA).

Disclosures

The authors have no financial conflicts of interest.

References

1. Angus, D. C., and T. van der Poll. 2013. Severe sepsis and septic shock. *N. Engl. J. Med.* 369: 840–851.
2. Martin, G. S., D. M. Mannino, S. Eaton, and M. Moss. 2003. The epidemiology of sepsis in the United States from 1979 through 2000. *N. Engl. J. Med.* 348: 1546–1554.
3. Mehrad, B., N. M. Clark, G. G. Zhanel, and J. P. Lynch, III. 2015. Antimicrobial resistance in hospital-acquired gram-negative bacterial infections. *Chest* 147: 1413–1421.
4. Jones, J. E., C. P. Causey, B. Knuckley, J. L. Slack-Noyes, and P. R. Thompson. 2009. Protein arginine deiminase 4 (PAD4): current understanding and future therapeutic potential. *Curr. Opin. Drug Discov. Devel.* 12: 616–627.
5. Koushik, S., N. Joshi, S. Nagaraju, S. Mahmood, K. Mudeenahally, R. Padmavathy, S. K. Jegatheesan, R. Mullangi, and S. Rajagopal. 2017. PAD4: pathophysiology, current therapeutics and future perspective in rheumatoid arthritis. *Expert Opin. Ther. Targets* 21: 433–447.
6. Nakashima, K., S. Arai, A. Suzuki, Y. Nariai, T. Urano, M. Nakayama, O. Ohara, K. Yamamura, K. Yamamoto, and T. Miyazaki. 2013. PAD4 regulates proliferation of multipotent haematopoietic cells by controlling c-myc expression. *Nat. Commun.* 4: 1836.
7. Ghari, F., A. M. Quirke, S. Munro, J. Kawalkowska, S. Picaud, J. McGouran, V. Subramanian, A. Muth, R. Williams, B. Kessler, et al. 2016. Citrullination-acetylation interplay guides E2F-1 activity during the inflammatory response. *Sci. Adv.* 2: e1501257.
8. Sharma, P., S. Azebi, P. England, T. Christensen, A. Møller-Larsen, T. Petersen, E. Batsché, and C. Muchardt. 2012. Citrullination of histone H3 interferes with HP1-mediated transcriptional repression. *PLoS Genet.* 8: e1002934.
9. Vossenaar, E. R., A. J. Zendman, W. J. van Venrooij, and G. J. Pruijn. 2003. PAD, a growing family of citrullinating enzymes: genes, features and involvement in disease. *BioEssays* 25: 1106–1118.
10. Wang, Y., M. Li, S. Stadler, S. Correll, P. Li, D. Wang, R. Hayama, L. Leonelli, H. Han, S. A. Grigoryev, et al. 2009. Histone hypercitrullination mediates chromatin decondensation and neutrophil extracellular trap formation. *J. Cell Biol.* 184: 205–213.
11. Li, P., M. Li, M. R. Lindberg, M. J. Kennett, N. Xiong, and Y. Wang. 2010. PAD4 is essential for antibacterial innate immunity mediated by neutrophil extracellular traps. *J. Exp. Med.* 207: 1853–1862.
12. McDonald, B., R. Urrutia, B. G. Yipp, C. N. Jenne, and P. Kubes. 2012. Intravascular neutrophil extracellular traps capture bacteria from the bloodstream during sepsis. *Cell Host Microbe* 12: 324–333.
13. Sørensen, O. E., and N. Borregaard. 2016. Neutrophil extracellular traps - the dark side of neutrophils. *J. Clin. Invest.* 126: 1612–1620.
14. Lewis, H. D., J. Liddle, J. E. Coote, S. J. Atkinson, M. D. Barker, B. D. Bax, K. L. Bicker, R. P. Bingham, M. Campbell, Y. H. Chen, et al. 2015. Inhibition of PAD4 activity is sufficient to disrupt mouse and human NET formation. *Nat. Chem. Biol.* 11: 189–191.
15. Rohrbach, A. S., D. J. Slade, P. R. Thompson, and K. A. Mowen. 2012. Activation of PAD4 in NET formation. *Front. Immunol.* 3: 360.
16. Konig, M. F., and F. Andrade. 2016. A critical reappraisal of neutrophil extracellular traps and NETosis mimics based on differential requirements for protein citrullination. *Front. Immunol.* 7: 461.
17. Neeli, I., and M. Radic. 2013. Opposition between PKC isoforms regulates histone deimination and neutrophil extracellular chromatin release. *Front. Immunol.* 4: 38.
18. Kenny, E. F., A. Herzig, R. Krüger, A. Muth, S. Mondal, P. R. Thompson, V. Brinkmann, H. V. Bernuth, and A. Zychlinsky. 2017. Diverse stimuli engage different neutrophil extracellular trap pathways. *Elife* 6: e24437.
19. McDonald, B., R. P. Davis, S. J. Kim, M. Tse, C. T. Esmon, E. Kolaczkowska, and C. N. Jenne. 2017. Platelets and neutrophil extracellular traps collaborate to promote intravascular coagulation during sepsis in mice. *Blood* 129: 1357–1367.
20. Martinod, K., T. A. Fuchs, N. L. Zitomersky, S. L. Wong, M. Demers, M. Gallant, Y. Wang, and D. D. Wagner. 2015. PAD4-deficiency does not affect bacteremia in polymicrobial sepsis and ameliorates endotoxemic shock. *Blood* 125: 1948–1956.
21. Douda, D. N., R. Jackson, H. Grasemann, and N. Palaniyar. 2011. Innate immune collectin surfactant protein D simultaneously binds both neutrophil extracellular traps and carbohydrate ligands and promotes bacterial trapping. *J. Immunol.* 187: 1856–1865.
22. Papayannopoulos, V., K. D. Metzler, A. Hakkim, and A. Zychlinsky. 2010. Neutrophil elastase and myeloperoxidase regulate the formation of neutrophil extracellular traps. *J. Cell Biol.* 191: 677–691.
23. Lefrançais, E., B. Mallavia, H. Zhuo, C. S. Calfee, and M. R. Looney. 2018. Maladaptive role of neutrophil extracellular traps in pathogen-induced lung injury. *JCI Insight* DOI: 10.1172/jci.insight.98178.
24. Narayana Moorthy, A., T. Narasaraju, P. Rai, R. Perumalsamy, K. B. Tan, S. Wang, B. Engelward, and V. T. Chow. 2013. In vivo and in vitro studies on the roles of neutrophil extracellular traps during secondary pneumococcal pneumonia after primary pulmonary influenza infection. *Front. Immunol.* 4: 56.
25. Achouiti, A., T. Vogl, C. F. Urban, M. Röhm, T. J. Hommes, M. A. van Zoelen, S. Florquin, J. Roth, C. van 't Veer, A. F. de Vos, and T. van der Poll. 2012. Myeloid-related protein-14 contributes to protective immunity in gram-negative pneumonia derived sepsis. *PLoS Pathog.* 8: e1002987.
26. de Stoppelaar, S. F., C. van 't Veer, T. A. M. Claushuis, B. J. A. Albersen, J. J. T. H. Roelofs, and T. van der Poll. 2014. Thrombocytopenia impairs host defense in gram-negative pneumonia-derived sepsis in mice. *Blood* 124: 3781–3790.
27. Boshuizen, M., J. H. Leopold, T. Zakharkina, H. H. Knobel, H. Weda, T. M. Nijsen, T. J. Vink, P. J. Sterk, M. J. Schultz, and L. D. Bos, MARS consortium. 2015. Levels of cytokines in broncho-alveolar lavage fluid, but not in plasma, are associated with levels of markers of lipid peroxidation in breath of ventilated ICU patients. *J. Breath Res.* 9: 036010.
28. Bone, R. C., R. A. Balk, F. B. Cerra, R. P. Dellinger, A. M. Fein, W. A. Knaus, R. M. H. Schein, and W. J. Sibbald, The ACCP/SCCM Consensus Conference Committee. American College of Chest Physicians/Society of Critical Care Medicine. 1992. Definitions for sepsis and organ failure and guidelines for the use of innovative therapies in sepsis. *Chest* 101: 1644–1655.
29. Klein Klouwenberg, P. M., D. S. Ong, L. D. Bos, F. M. de Beer, R. T. van Hooijdonk, M. A. Huson, M. Straat, L. A. van Vught, L. Wieske, J. Horn, et al. 2013. Interobserver agreement of centers for disease control and prevention criteria for classifying infections in critically ill patients. *Crit. Care Med.* 41: 2373–2378.
30. Levy, M. M., M. P. Fink, J. C. Marshall, E. Abraham, D. Angus, D. Cook, J. Cohen, S. M. Opal, J. L. Vincent, and G. Ramsay, International Sepsis Definitions Conference. 2003. 2001 SCCM/ESICM/ACCP/ATS/SIS International sepsis definitions conference. *Intensive Care Med.* 29: 530–538.
31. van Zoelen, M. A. D., S. Florquin, J. C. M. Meijers, R. de Beer, A. F. de Vos, O. J. de Boer, and T. van der Poll. 2008. Platelet-activating factor receptor contributes to host defense against *Pseudomonas aeruginosa* pneumonia but is not essential for the accompanying inflammatory and procoagulant response. *J. Immunol.* 180: 3357–3365.
32. Anas, A. A., M. H. van Lieshout, T. A. Claushuis, A. F. de Vos, S. Florquin, O. J. de Boer, B. Hou, C. Van't Veer, and T. van der Poll. 2016. Lung epithelial MyD88 drives early pulmonary clearance of *Pseudomonas aeruginosa* by a flagellin dependent mechanism. *Am. J. Physiol. Lung Cell. Mol. Physiol.* 311: L219–L228.
33. Leendertse, M., R. J. Willems, I. A. Giebelen, J. J. Roelofs, M. J. Bonten, and T. van der Poll. 2009. Neutrophils are essential for rapid clearance of *Enterococcus* faecium in mice. *Infect. Immun.* 77: 485–491.
34. Zeerleder, S., B. Zwart, W. A. Wuillemin, L. A. Aarden, A. B. Groeneveld, C. Caliezi, A. E. van Nieuwenhuijze, G. J. van Mierlo, A. J. Eerenberg, B. Lämmle, and C. E. Hack. 2003. Elevated nucleosome levels in systemic inflammation and sepsis. *Crit. Care Med.* 31: 1947–1951.
35. de Stoppelaar, S. F., T. A. Claushuis, M. P. Jansen, B. Hou, J. J. Roelofs, C. van 't Veer, and T. van der Poll. 2015. The role of platelet MyD88 in host response during gram-negative sepsis. *J. Thromb. Haemost.* 13: 1709–1720.
36. Brinkmann, V., U. Abu Abed, C. Goosmann, and A. Zychlinsky. 2016. Immunodetection of NETs in paraffin-embedded tissue. *Front. Immunol.* 7: 513.
37. de Boer, O. J., X. Li, H. Goebel, and A. C. van der Wal. 2016. Nuclear smears observed in H&E-stained thrombus sections are neutrophil extracellular traps. *J. Clin. Pathol.* 69: 181–182.
38. Stokman, G., J. Kers, Ü. Yapici, J. J. Hoelbeek, N. Claessen, O. J. de Boer, M. G. Netea, L. Hilbrands, F. J. Bemelman, I. J. Ten Berge, and S. Florquin. 2016. Predominant tubular interleukin-18 expression in polyomavirus-associated nephropathy. *Transplantation* 100: e88–e95.
39. Rijneveld, A. W., S. Weijer, S. Florquin, C. T. Esmon, J. C. Meijers, P. Speelman, P. H. Reitsma, H. Ten Cate, and T. van der Poll. 2004. Thrombomodulin mutant mice with a strongly reduced capacity to generate activated protein C have an unaltered pulmonary immune response to respiratory pathogens and lipopolysaccharide. *Blood* 103: 1702–1709.
40. Kolaczkowska, E., C. N. Jenne, B. G. Surewaard, A. Thanabalasuriar, W. Y. Lee, M. J. Sanz, K. Mowen, G. Opdenakker, and P. Kubes. 2015. Molecular mechanisms of NET formation and degradation revealed by intravital imaging in the liver vasculature. *Nat. Commun.* 6: 6673.
41. Gould, T. J., T. T. Vu, L. L. Swystun, D. J. Dwivedi, S. H. Mai, J. I. Weitz, and P. C. Liaw. 2014. Neutrophil extracellular traps promote thrombin generation through platelet-dependent and platelet-independent mechanisms. *Arterioscler. Thromb. Vasc. Biol.* 34: 1977–1984.
42. Knight, J. S., V. Subramanian, A. A. O'Dell, S. Yalavarthi, W. Zhao, C. K. Smith, J. B. Hodgin, P. R. Thompson, and M. J. Kaplan. 2015. Peptidylarginine deiminase inhibition disrupts NET formation and protects against kidney, skin and vascular disease in lupus-prone MRL/lpr mice. *Ann. Rheum. Dis.* 74: 2199–2206.
43. Martinod, K., M. Demers, T. A. Fuchs, S. L. Wong, A. Brill, M. Gallant, J. Hu, Y. Wang, and D. D. Wagner. 2013. Neutrophil histone modification by peptidylarginine deiminase 4 is critical for deep vein thrombosis in mice. *Proc. Natl. Acad. Sci. USA* 110: 8674–8679.
44. Bawadekar, M., D. Shim, C. J. Johnson, T. F. Warner, R. Rebernick, D. Damgaard, C. H. Nielsen, G. J. M. Pruijn, J. E. Nett, and M. A. Shelef. 2017. Peptidylarginine deiminase 2 is required for tumor necrosis factor alpha-induced citrullination and arthritis, but not neutrophil extracellular trap formation. *J. Autoimmun.* 80: 39–47.

45. Khan, M. A., and N. Palaniyar. 2017. Transcriptional firing helps to drive NETosis. *Sci. Rep.* 7: 41749.
46. Douda, D. N., M. A. Khan, H. Grasemann, and N. Palaniyar. 2015. SK3 channel and mitochondrial ROS mediate NADPH oxidase-independent NETosis induced by calcium influx. *Proc. Natl. Acad. Sci. USA* 112: 2817–2822.
47. Yang, S., H. Qi, K. Kan, J. Chen, H. Xie, X. Guo, and L. Zhang. 2017. Neutrophil extracellular traps promote hypercoagulability in patients with sepsis. *Shock.* 47: 132–139.
48. Kaufman, T., D. Magosevich, M. C. Moreno, M. A. Guzman, L. P. D'Atri, A. Carestia, M. E. Fandiño, C. Fondevila, and M. Schattner. 2017. Nucleosomes and neutrophil extracellular traps in septic and burn patients. *Clin. Immunol.* 183: 254–262.
49. Schuster, B. S., J. S. Suk, G. F. Woodworth, and J. Hanes. 2013. Nanoparticle diffusion in respiratory mucus from humans without lung disease. *Biomaterials* 34: 3439–3446.
50. Sarris, P. F., C. Zoumadakis, N. J. Panopoulos, and E. V. Scoulica. 2011. Distribution of the putative type VI secretion system core genes in *Klebsiella* spp. *Infect. Genet. Evol.* 11: 157–166.
51. Liu, L., M. Ye, X. Li, J. Li, Z. Deng, Y. F. Yao, and H. Y. Ou. 2017. Identification and characterization of an antibacterial type VI secretion system in the Carbapenem-resistant strain *Klebsiella pneumoniae* HS11286. *Front. Cell. Infect. Microbiol.* 7: 442.
52. Witalison, E. E., P. R. Thompson, and L. J. Hofseth. 2015. Protein arginine deiminases and associated citrullination: physiological functions and diseases associated with dysregulation. *Curr. Drug Targets* 16: 700–710.
53. Jang, B., H. W. Kim, J. S. Kim, W. S. Kim, B. R. Lee, S. Kim, H. Kim, S. J. Han, S. J. Ha, and S. J. Shin. 2015. Peptidylarginine deiminase inhibition impairs Toll-like receptor agonist-induced functional maturation of dendritic cells, resulting in the loss of T cell-proliferative capacity: a partial mechanism with therapeutic potential in inflammatory settings. *J. Leukoc. Biol.* 97: 351–362.
54. Fuchs, T. A., U. Abed, C. Goosmann, R. Hurwitz, I. Schulze, V. Wahn, Y. Weinrauch, V. Brinkmann, and A. Zychlinsky. 2007. Novel cell death program leads to neutrophil extracellular traps. *J. Cell Biol.* 176: 231–241.
55. Hakkim, A., T. A. Fuchs, N. E. Martinez, S. Hess, H. Prinz, A. Zychlinsky, and H. Waldmann. 2011. Activation of the Raf-MEK-ERK pathway is required for neutrophil extracellular trap formation. *Nat. Chem. Biol.* 7: 75–77.
56. Remijsen, Q., T. Vanden Berghe, E. Wirawan, B. Asselbergh, E. Parthoens, R. De Rycke, S. Noppen, M. Delforge, J. Willems, and P. Vandenabeele. 2011. Neutrophil extracellular trap cell death requires both autophagy and superoxide generation. *Cell Res.* 21: 290–304.
57. Keshari, R. S., A. Verma, M. K. Barthwal, and M. Dikshit. 2013. Reactive oxygen species-induced activation of ERK and p38 MAPK mediates PMA-induced NETs release from human neutrophils. *J. Cell. Biochem.* 114: 532–540.
58. Pilsczek, F. H., D. Salina, K. K. Poon, C. Fahey, B. G. Yipp, C. D. Sibley, S. M. Robbins, F. H. Green, M. G. Surette, M. Sugai, et al. 2010. A novel mechanism of rapid nuclear neutrophil extracellular trap formation in response to *Staphylococcus aureus.* *J. Immunol.* 185: 7413–7425.
59. Martinod, K., T. Witsch, K. Farley, M. Gallant, E. Remold-O'Donnell, and D. D. Wagner. 2016. Neutrophil elastase-deficient mice form neutrophil extracellular traps in an experimental model of deep vein thrombosis. *J. Thromb. Haemost.* 14: 551–558.
60. Luo, Y., K. Arita, M. Bhatia, B. Knuckley, Y. H. Lee, M. R. Stallcup, M. Sato, and P. R. Thompson. 2006. Inhibitors and inactivators of protein arginine deiminase 4: functional and structural characterization. *Biochemistry* 45: 11727–11736.
61. Hemmers, S., J. R. Teijaro, S. Arandjelovic, and K. A. Mowen. 2011. PAD4-mediated neutrophil extracellular trap formation is not required for immunity against influenza infection. *PLoS One* 6: e22043.
62. Zhao, T., B. Pan, H. B. Alam, B. Liu, R. T. Bronson, Q. Deng, E. Wu, and Y. Li. 2016. Protective effect of Cl-amidine against CLP-induced lethal septic shock in mice. *Sci. Rep.* 6: 36696.
63. Li, Y., Z. Liu, B. Liu, T. Zhao, W. Chong, Y. Wang, and H. B. Alam. 2014. Citrullinated histone H3: a novel target for the treatment of sepsis. *Surgery* 156: 229–234.
64. Biron, B. M., C. S. Chung, X. M. O'Brien, Y. Chen, J. S. Reichner, and A. Ayala. 2017. Cl-amidine prevents histone 3 citrullination and neutrophil extracellular trap formation, and improves survival in a murine sepsis model. *J. Innate Immun.* 9: 22–32.
65. Claushuis, T. A., S. F. de Stoppelaar, I. Stroo, J. J. Roelofs, R. Ottenhoff, T. van der Poll, and C. Van't Veer. 2017. Thrombin contributes to protective immunity in pneumonia-derived sepsis via fibrin polymerization and platelet-neutrophil interactions. *J. Thromb. Haemost.* 15: 744–757.
66. Claushuis, T. A. M., A. F. de Vos, B. Nieswandt, L. Boon, J. J. T. H. Roelofs, O. J. de Boer, C. van 't Veer, and T. van der Poll. 2018. Platelet glycoprotein VI aids in local immunity during pneumonia-derived sepsis caused by gram-negative bacteria. *Blood* 131: 864–876.